Optical detection of electron-nuclear double resonance for a donor in oxygen-doped GaP

D. Y. Jeon, J. F. Donegan, and G. D. Watkins
Sherman Fairchild Laboratory and Physics Department,
Lehigh University, Bethlehem, Pennsylvania 18015
(Received 15 August 1988)

Optical detection of electron-nuclear double resonance (ODENDOR) has been used in a study of an optically detected magnetic resonance spectrum previously assigned to the shallow effective-mass-like $1S(E)$ state of the substitutional oxygen donor in GaP. The ODENDOR spectra were observed via photoluminescence transitions which are known to be oxygen related. Hyperfine interactions with several shells of both P and Ga neighbors were observed showing that the defect center is on the P sublattice and has full T_d (tetrahedral) symmetry. A substantial hyperfine interaction was observed on the Ga sublattice inconsistent with an effective-mass-like state made up from the lowest X_1 conduction-band valleys. Further, the full tetrahedral symmetry of the defect as deduced from the ODENDOR spectra reveals an A_1 state not consistent with the $1S(E)$ state believed to be involved in the electron-capture luminescence transition. Analysis of the defect wave-function distribution gives a binding energy of about 0.22 eV.

I. INTRODUCTION

The oxygen donor in GaP is surely one of the most studied systems in defect physics. In the pioneering work of Dean and his co-workers[1,2] two new photoluminescence (PL) transitions were found when GaP was doped with oxygen. One of these was identified as arising from distant donor-acceptor pair (DAP) recombination giving the energy-level position of the single donor state $(0/+)$ of oxygen in GaP at $E_c-0.893$ eV. The second transition, labeled an electron-capture (EC) PL was proposed to occur between an excited effective-mass-like $1S(E)$ state at $E_c-0.052$ eV and the ground $1S(A_1)$ state of the neutral oxygen donor. Dean *et al.*[2] proposed that the large splitting of the $1S(E)$ and $1S(A_1)$ states resulted from a large central cell effect at the donor. In Fig. 1(a) we have summarized Dean's model for the role of oxygen in GaP. In 1973, photocapacitance measurements on GaP:O showed that there was an additional deep acceptor level $(-/0)$ associated with oxygen, also at $\sim E_c-0.9$ eV.[3,4]

The model proposed by Dean has been challenged by Morgan,[5] who suggested a new "weak-bonding" mechanism to explain the electronic properties of oxygen in GaP. In an extensive review of the spectroscopic data obtained on GaP:O, Dean[6] reviewed both his and Morgan's models and concluded that his original model was in fact the correct one. Magnetic resonance studies which have often helped differentiate between models have not been very effective on GaP:O. One reason for this is that the magnetic isotope of oxygen, ^{17}O, is only 0.04% abundant making a direct correlation between magnetic resonance signals and the presence of oxygen or no presence of oxygen in the defect very difficult.

Electron-paramagnetic-resonance studies in oxygen-doped GaP were first carried out in 1970 by Toyotomi *et al.*[7] They observed an isotropic resonance with $g=1.997$ whose strength was proportional to the oxygen concentration in their samples. In 1979, optically detected magnetic resonance (ODMR) was reported for GaP:O by Gal *et al.*[8] They observed two distinct spectra, an isotropic resonance with $g\simeq 2$ which showed no sign of resolved hyperfine structure, and a triplet $(S=1)$ resonance showing a strong resolved hyperfine interaction with a single Ga nucleus. From this and subsequent Zeeman and stress studies,[9] the triplet spectrum was assigned to an Auger process between O^- and O^0. Recently, however, Lee[10] and Godlewski and Monemar[11] have suggested that this interpretation is not correct. These authors suggest that the spectrum is related to the Ga interstitial (Ga_i) defect. An optical detection of electron-nuclear double resonance (ODENDOR) study of this triplet system will be published elsewhere.[12]

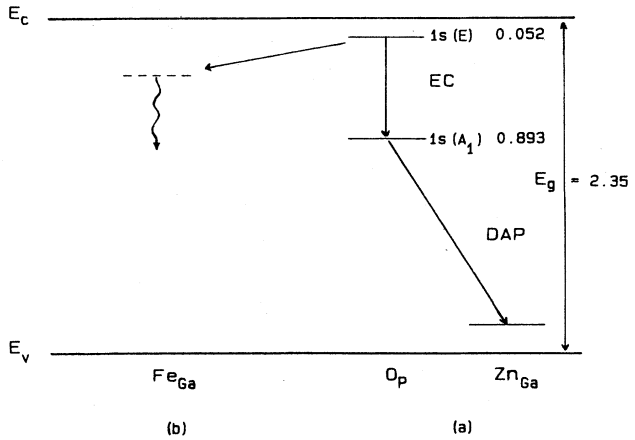

FIG. 1. (a) The model proposed by Dean *et al.* (Refs. 1 and 2) for the role of neutral oxygen in GaP. (b) The model of Lee *et al.* (Ref. 13) for the origin of the quenching $g\sim 2$ ODMR resonance in GaP:O,Fe. All numerical values are in units of eV.

The isotropic ODMR resonance is the subject of the present study. Lee *et al.*[13] proposed that the $g \simeq 2$ resonance occurs in the shallow effective-mass-like state of the excited neutral oxygen donor. In their case they provided evidence that this $g \simeq 2$ resonance serves to quench the two oxygen-related luminescence bands as a result of a competitive spin-dependent recombination process between the excited $1S(E)$ oxygen state and Fe impurities. The rather long lifetime of the EC PL, $\sim 10\ \mu$s, makes it possible for the excited state to lose its electron by transfer to a deep level. The model of Lee *et al.*[13] for this transfer process is shown in Fig. 1(b). In an attempt to test if this resonance is indeed due to the oxygen donor, we have undertaken this ODENDOR study.

II. EXPERIMENTAL DETAILS

The sample used in this investigation was a liquid-encapsulated Czochralski-grown GaP crystal, supplied by K. M. Lee. Boric oxide (B_2O_3) had been added to the melt during growth to achieve oxygen doping. The sample dimensions were $1 \times 1 \times 1.5$ mm^3.

PL, ODMR, and ODENDOR experiments were all carried out at 1.7 K in an Oxford Instruments SM-4 superconducting magnet optical cryostat. The sample was mounted in a 35-GHz TE_{011} mode microwave cavity designed in the form of concentric rings for optical access.[14] Luminescence was excited by ~ 40 mW of the 514.5-nm line of an Ar^+ laser and detected by either a North-Coast EO-817P Ge detector or an EG&G UV250 Si photodiode. ODMR spectra were recorded by monitoring changes in the PL intensity synchronous with on-off amplitude modulation of the microwaves. In order to determine the spectral dependence of the ODMR signals, the PL was dispersed by a Jarrell-Ash 82-487 0.25-m monochromator prior to detection. For the ODENDOR studies, a two-turn coil was installed in the cavity such that its magnetic field axis was perpendicular to both the static and microwave magnetic fields. cw radio frequency power was supplied to the coil from a Fluke 6060B frequency synthesizer amplified by an ENI 3100LA solid-state amplifier. The static magnetic field was tuned to the $g \simeq 2$ resonance and changes in the ODMR signal intensity were recorded as the radiofrequency was swept. The frequency sweep of the synthesizer was computer controlled with signal averaging being performed as necessary.

III. EXPERIMENTAL RESULTS

Figure 2(a) shows the near-infrared PL spectrum of the GaP:O sample taken with a resolution of ~ 20 nm. The two bands correspond to the transitions originally observed by Dean *et al.*[1,2] The band centered at 1050 nm is the DAP PL transition between the deep oxygen donor and an unknown shallow acceptor. The structured band centered at 1570 nm is the EC PL transition. The ODMR spectrum recorded with the magnetic field $\mathbf{B}\|[110]$ is shown in Fig. 3. This spectrum is identical to that first observed by Gal *et al.*[8] We are concerned here with the quenching resonance at 1.24 T (i.e., the PL intensity decreases at resonance) with $g = 1.998$. This signal

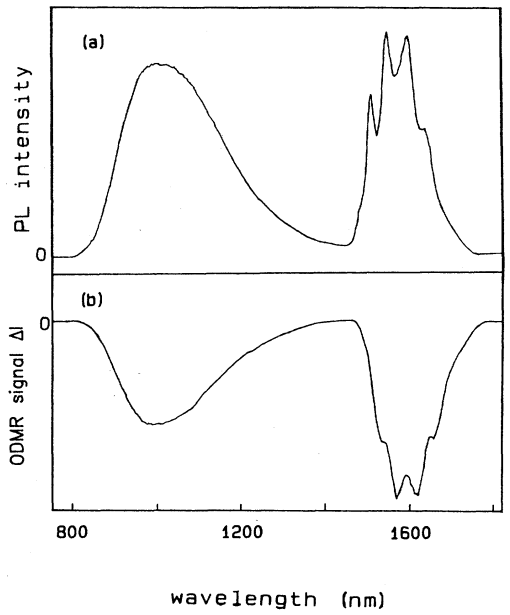

FIG. 2. (a) The near-infrared PL spectrum obtained from GaP:O at $T = 1.7$ K. (b) The spectral dependence of the negative $g = 1.998$ ODMR resonance at $T = 1.7$ K. The spectra are uncorrected for the system response.

is isotropic, it has a full width at half maximum of 120 G and shows no sign of resolved hyperfine structure. The spectral dependence of this resonance is shown in Fig. 2(b) where we can see that both oxygen-related PL bands are quenched by the resonance.

A full-sweep ODENDOR spectrum of the $g = 1.998$ resonance taken with $\mathbf{B}\|[100]$ is shown in Fig. 4. The nuclear spin Hamiltonian appropriate to this system and accurate to first order in $A_i/g\mu_B B$ and $Q_i'/g\mu_B B$ is

$$\mathcal{H}_n = \sum \mathbf{I}_i \cdot \left[\tilde{\mathbf{A}}_i \frac{M_s}{B} - \frac{\mu_i}{I_i} \right] \cdot \mathbf{B} + \sum \mathbf{I}_i \cdot \tilde{\mathbf{Q}}_i' \cdot \mathbf{I}_i \qquad (1)$$

for the state described by the azimuthal quantum number

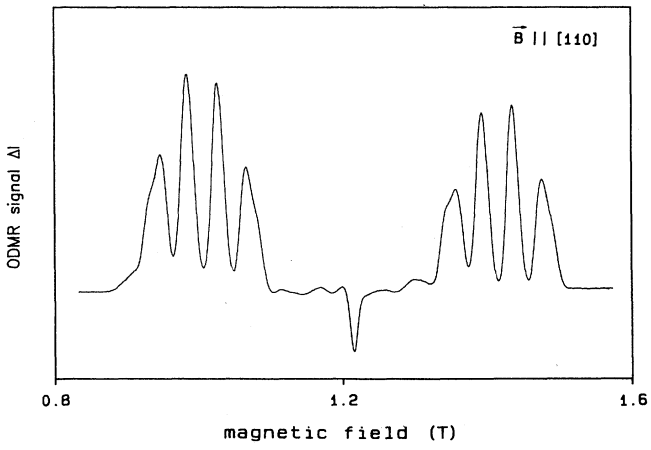

FIG. 3. The ODMR spectrum from GaP:O with $\mathbf{B}\|[110]$ at $\nu = 35.0$ GHz and $T = 1.7$ K.

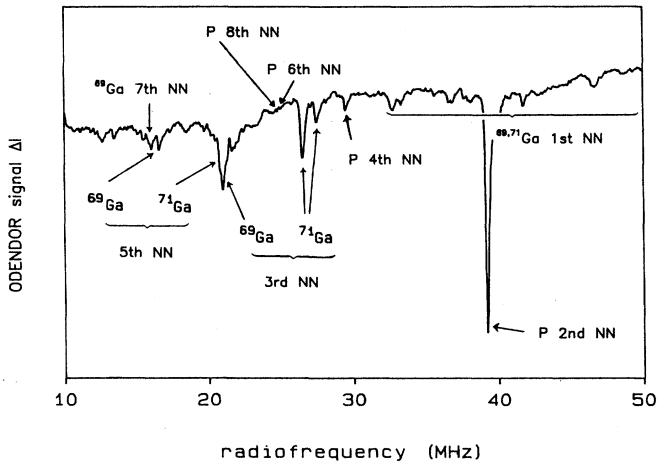

FIG. 4. The ODENDOR spectrum of the $g=1.998$ quenching ODMR line with $\mathbf{B}\|[100]$ at $B=1.24$ T and $T=1.7$ K.

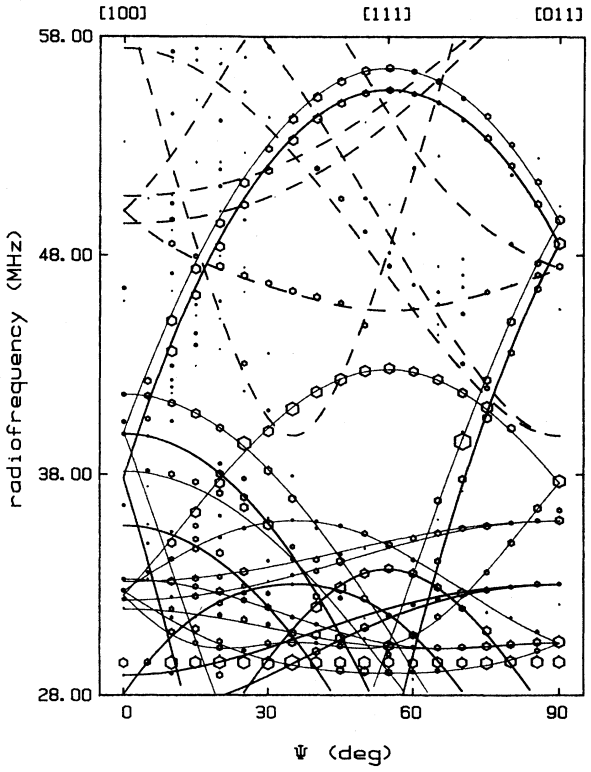

FIG. 5. The angular dependence of the first-nearest-neighbor Ga ODENDOR lines, $\mathbf{B}\perp[01\bar{1}]$. The hexagons are the experimental data and the lines are a theoretical fit to Eq. (1). (^{69}Ga allowed $\Delta m_I=\pm1$ transitions, heavy solid lines; ^{69}Ga $\Delta m_I=\pm2$ transitions, heavy dashed lines; ^{71}Ga $\Delta m_I=\pm1$ transitions, light solid lines.)

M_s. The first term contains the magnetic hyperfine and nuclear Zeeman interactions and the second term the quadrupole interaction appropriate for $I_i>\frac{1}{2}$. Although Fig. 4 contains a large number of lines, the nucleus involved in each could be identified by measuring the nuclear gyromagnetic ratio, μ_i/I_i, from the dependence of the transition energy on the magnetic field $\mathbf{B}$ [Eq. (1)]. All of the ODENDOR lines are found to be accounted for by the two Ga nuclei, ^{69}Ga and ^{71}Ga, and the single ^{31}P nucleus.

An angular dependence study was undertaken and in Figs. 5–8 the angular variation under higher resolution for four shells of neighbors are shown. In these diagrams the data are represented by hexagons whose area is in proportion to the strength of the ODENDOR signal as determined automatically by a computer algorithm. The spin Hamiltonian parameters for these four shells are given in Table I; the fit to the experimental data is shown in Figs. 5–8. The principal axis system used in analyzing the angular dependencies is shown in Fig. 9.

All of the data shown in Fig. 5 (except for the nearly isotropic P signal at $\sim$29.5 MHz) are accounted for by the two gallium isotopes. The fit to the data was obtained by matrix diagonalization of Eq. (1). The fit is excellent, the ratios of the hyperfine and quadrupole interactions for the two isotopes matching the known nuclear moment ratios[15] [$\mu(^{69}\text{Ga})/\mu(^{71}\text{Ga})=0.7875$; $Q(^{69}\text{Ga})/Q(^{71}\text{Ga})=1.587$] within experimental accuracy. We note that normally forbidden $\Delta m_I=\pm2$ transitions were observed for the ^{69}Ga isotope (which has the larger quadrupole moment) and are indicated by the heavy dashed lines in Fig. 5. Despite having axial symmetry all the four branches for each $\Delta m_I=\pm1$ and $\Delta m_I=\pm2$ transitions do not collapse to a single point along [100]. This is the result of a slight tilting of the sample, $\sim2°$, out of the $(01\bar{1})$ plane, the small size of the sample making exact alignment difficult. This tilting has been included in the theoretical fit.

The spectrum in Fig. 6 is due to ^{31}P, its symmetry being monoclinic (C_{1h}). In Fig. 7 we show a spectrum from ^{71}Ga. Its symmetry is also monoclinic (C_{1h}). A spectrum for ^{69}Ga in the same shell, not shown, is also observed, with identical symmetry at lower frequencies, but scaled by $\mu(^{69}\text{Ga})/\mu(^{71}\text{Ga})$ and $Q(^{69}\text{Ga})/Q(^{79}\text{Ga})$. The fit to these spectra required only perturbation terms to first order in Q_i/A_i. Figure 8 shows another ^{31}P spectrum; this time its symmetry is orthorhombic (C_{2v}). The tilting of the crystal mentioned above has also been included in these theoretical fits. Finally, two additional P and Ga shells at lower frequencies have also been identified and are indicated in Fig. 4. Although weak in intensity, signal averaging makes them clearly visible. For these, the anisotropy was small and only the isotropic part of the hyperfine interaction was determined. Table I summarizes the results for all eight shells. Equation (1) predicts two sets of ENDOR transitions, one for each of the $M_S=\pm\frac{1}{2}$ states. However, in our case we observe only one set of transitions, the high-frequency set, and therefore we were unable to determine the relative sign of A_i and Q_i'. Measurements of the nuclear gyromagnetic ratio along principal directions show that the A_i components all have the same sign.

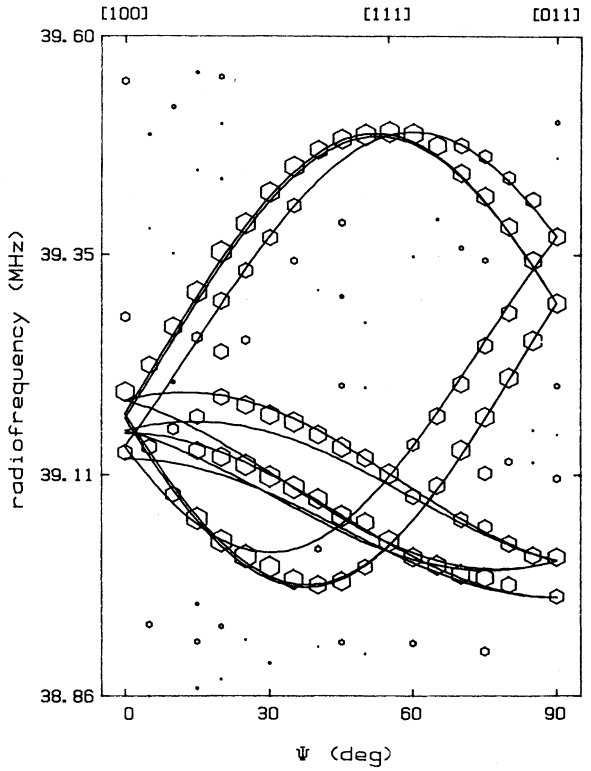

FIG. 6. The angular dependence of the second-nearest-neighbor P ODENDOR lines, $\mathbf{B}\perp[01\bar{1}]$. The hexagons are the experimental data and the lines are a theoretical fit to the first term in Eq. (1).

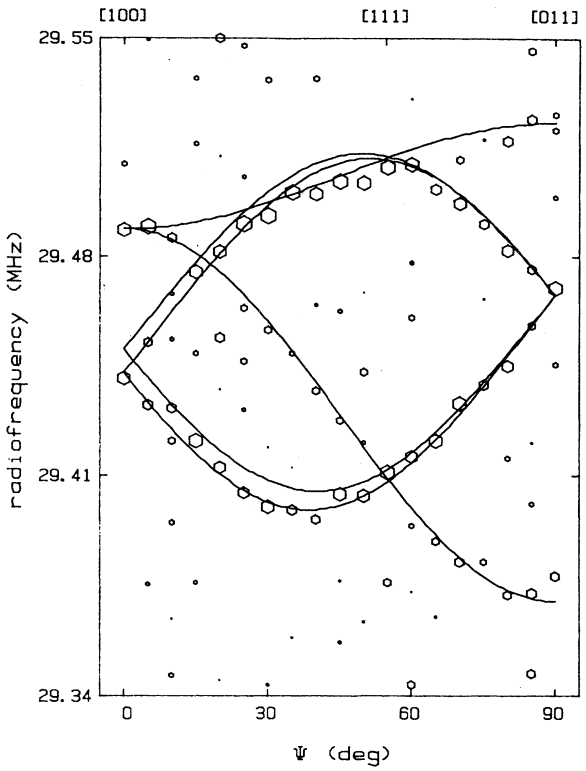

FIG. 8. The angular dependence of the fourth-nearest-neighbor P ODENDOR lines, $\mathbf{B}\perp[01\bar{1}]$.

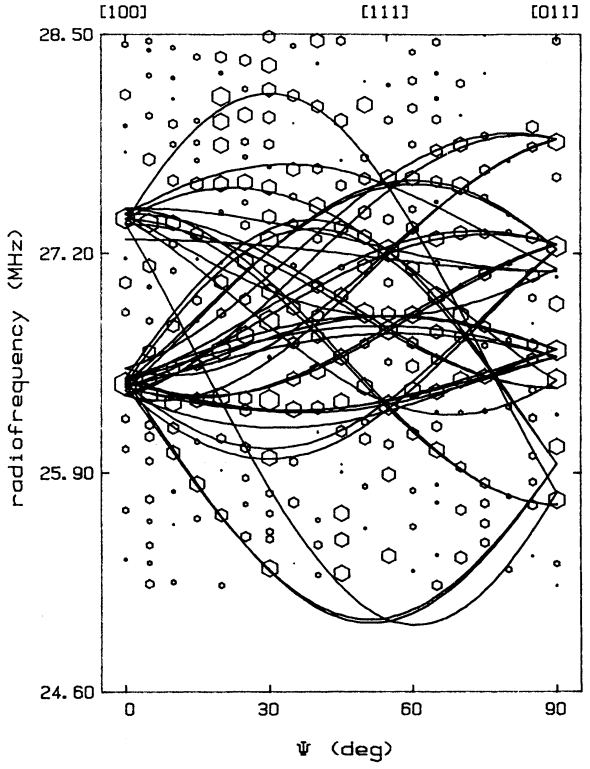

FIG. 7. The angular dependence of the third-nearest-neighbor ^{71}Ga ODENDOR lines, $\mathbf{B}\perp[01\bar{1}]$.

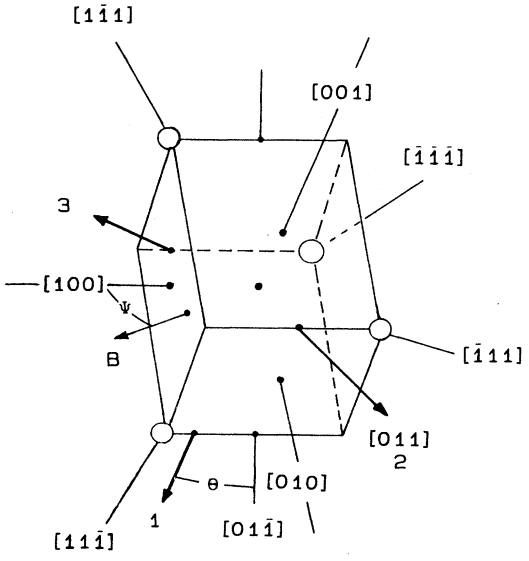

FIG. 9. The principal axes of the $\tilde{\mathbf{g}}$, $\tilde{\mathbf{A}}$, and $\tilde{\mathbf{Q}}$ tensors used in our analysis.

TABLE I. Spin Hamiltonian parameters for the shells of neighbors analyzed. The principal axes are defined in Fig. 9.

Atomic site	$\|A_1\|$	$\|A_2\|$	$\|A_3\|$	(MHz)	Q_1	Q_2	Q_3
^{71}Ga 1NN	53.27	26.01	26.01		± 4.60	∓ 2.30	∓ 2.30
^{69}Ga 1NN	41.95 $\theta=35.26°$	20.48	20.48		± 7.30 $\theta=35.26°$	∓ 3.65	∓ 3.65
^{71}Ga 3NN	22.90 $\theta=67.8°$	20.53	20.21		± 0.20 $\theta=54.8°$	± 0.23	∓ 0.43
^{69}Ga 5NN	7.56	7.56	7.56				
^{69}Ga 7NN	6.68	6.68	6.68				
^{31}P 2NN	36.19 $\theta=30.0°$	35.19	35.26				
^{31}P 4NN	16.20 $\theta=90.0°$	15.96	16.26				
^{31}P 6NN	6.72	6.72	6.72				
^{31}P 8NN	6.02	6.02	6.02				

IV. DISCUSSION

A. Wave function for an effective-mass-like state

Before going on to the interpretation of the ODENDOR data, let us consider the form of the wave function expected for a shallow effective-mass-like state of a donor in GaP, in our case the excited $1S(E)$ state of the oxygen donor at $E_c-0.052$ eV.

GaP is an indirect-band-gap semiconductor. The conduction-band minima are very close to the Brillouin-zone-edge X point.[16] If the donor under study is effective-mass-like, then the wave function of the donor electron in its $1S$ state can be approximately represented by a linear combination of the three Bloch states corresponding to the three equivalent X_1 minima of the conduction band, modulated by a slowly varying envelope function of $1S$ symmetry. That is

$$\psi(\mathbf{r})=\sum_{j=1}^{3}\alpha_j F^{(j)}(\mathbf{r})u^j(\mathbf{r})\exp(i\mathbf{k}_0^j\cdot\mathbf{r})\ , \tag{2}$$

where j refers to the different minima, $u^{(j)}(\mathbf{r})\exp(i\mathbf{k}_0^j\cdot\mathbf{r})$ is the Bloch function of the jth minimum at $k_0\simeq 2\pi/a$, $F^{(j)}(\mathbf{r})$ is a $1S$ hydrogenlike envelope function obtained by solving an effective-mass Schrödinger equation, and α_j is a weighting factor for each minimum. It has been established experimentally that at the X_1 minimum the conduction-band wave function is maximum on the P sites with nodes on the Ga sites.[17] $|\psi(r_m)|^2$, the amplitude squared of the wave function at the nucleus of atom site m, should therefore be zero for atoms on the Ga sublattice. The fact that considerable hyperfine interactions are observed at the Ga sites is the first strong indication that the donor under study is not shallow effective-mass-like.

B. Assignment of the ODENDOR spectra

The first step in the interpretation of the ODENDOR data is to attempt to order the various shells around the defect. For a true effective-mass state of the form of Eq. (2), this is not straightforward because the $\exp(i\mathbf{k}_0^j\cdot\mathbf{r})$ terms of the three X_1 minima will interfere with each other and $|\psi(\mathbf{r}_m)|^2$ will not decrease monotonically with increasing $\mathbf{r}_m$, but will rather show oscillations from one neighbor shell to the other.[18] However, since in our case we observe a considerable hyperfine interaction on the Ga sublattice the defect wave function cannot be strictly effective-mass-like. As a result, we will tentatively order shells that cannot be distinguished by symmetry by decreasing $|\psi(r_m)|^2$. We will return to a critical evaluation of this assumption later.

The first-nearest-neighbor shell is expected to have [111] axial (C_{3v}) symmetry. Therefore, we assign the Ga spectrum in Fig. 5 to the first-nearest-neighbor shell around the defect. This establishes that the defect is centered on the P sublattice. The second- (P), third- (Ga), and fourth- (P) nearest-neighbor shells must therefore have C_{1h}, C_{1h}, C_{2v} symmetry, respectively, and so the spectrum in Fig. 6 is assigned to the second-nearest-neighbor shell, that in Fig. 7 to the third-nearest-neighbor shell, and that in Fig. 8 to the fourth-nearest-neighbor shell. The remaining two Ga spectra are tentatively assigned to the fifth- and seventh-nearest-neighbor shells, the two P spectra to the sixth- and eighth-nearest-neighbor shells, each in order of decreasing hyperfine interaction. These assignments are also included in Table I.

The ODENDOR lines of each shell are rather narrow having a full width at half maximum of about 0.05 MHz. However, a $1S(E)$ state is doubly degenerate and strains would mix these two levels and considerably broaden the ODENDOR lines. This provides strong additional evidence that the ODMR resonance does not occur in the $1S(E)$ state of the oxygen donor.

C. LCAO analysis

One method for analyzing the wave-function distribution of the unpaired electron on the defect is by the linear combination of atomic orbitals (LCAO) approximation. The unpaired electron is represented by a linear combination of atomic orbitals centered on the atoms near the defect

$$\psi=\sum_j \eta_j\phi_j \ , \tag{3}$$

where η_j^2 is the amount of the electron distribution at the jth atomic site. The atomic orbital is in turn approximated by a combination of s and p valence orbitals

$$\phi_j=\alpha_j(\phi_{ns})_j+\beta_j(\phi_{np})_j \ , \tag{4}$$

where α_j^2 is the fraction of s orbital and β_j^2 the fraction of p orbital, in ϕ_j. In the approximation that the hyperfine interaction at the jth site is determined primarily by ϕ_j, the interaction is axially symmetric along the p-orbital axis and can be written[19]

$$\begin{aligned}(A_\parallel)_j&=a_j+2b_j \ ,\\ (A_\perp)_j&=a_j-b_j \ .\end{aligned} \tag{5}$$

The isotropic term a_j arises from the Fermi-contact interaction

$$a_j=\left[\frac{16\pi}{3}\right]\left[\frac{\mu_j}{I_j}\right]\mu_B\alpha_j^2\eta_j^2|\phi_{ns}(0)|^2 \ , \tag{6}$$

where μ_j is the magnetic moment and I_j the spin of the jth nucleus, while the anisotropic term b results from the dipole-dipole interaction averaged over the electronic wave function and given by

$$b_j=\frac{4}{5}\left[\frac{\mu_j}{I_j}\right]\mu_B\beta_j^2\eta_j^2\langle r_{np}^{-3}\rangle_j \ . \tag{7}$$

The free-ion values for ^{31}P were taken as $a=11\,146$ MHz, and $b=310$ MHz.[19] The values for ^{69}Ga were estimated using recent self-consistent Hartree-Fock calculations[20] and are $a=7430$ MHz and $b=148$ MHz. From these the molecular wave-function coefficients (α_j^2, β_j^2, and η_j^2) were calculated from the observed hyperfine parameters, a_j and b_j. The results are given in Table II. By multiplying η_j^2 by the number of equivalent nearest-neighbor sites, N, the total fraction of the wave function for each near-neighbor shell is determined. From Table II we see that, about 40% of the unpaired electron wave function is accounted for over the eight nearest-neighbor shells observed.

D. Envelope-function analysis

An alternative method of analyzing the defect wave function is to consider it as made up of a smoothly varying envelope function which is orthogonalized to the filled cores of the lattice atoms. The advantage of this approach is that it can serve as a guide to estimate the binding energy of the defect.

Following the method of Gourary and Adrian,[21,22] an "envelope function" $\Phi(\mathbf{r})$ which describes the average spatial distribution of the one-electron wave function is constructed. In a separate step, this envelope function is made orthogonal to the one-electron wave functions ϕ_i^α, representing all of the core orbitals (α) at each of the ith atomic sites. The unpaired electron wave function may then be written as

$$\psi(\mathbf{r})=N\left[\Phi(\mathbf{r})-\sum_{i,\alpha}\phi_i^\alpha\langle\phi_i^\alpha|\Phi\rangle\right] \ , \tag{8}$$

where N is a normalization constant. Gourary and Adrian[21,22] obtained the value of the electron density at the nucleus $|\psi(\mathbf{r}_i)|^2$ of the ith ion by multiplying the value of the envelope function $|\Phi(\mathbf{r}_i)|^2$ at this point by an amplification factor G, that roughly depends only on the nature of the ion. In this way, the isotropic hyperfine constants measured with magnetic resonance techniques could be used to estimate the value of the envelope function at each of the lattice points.

In Eq. (8), the admixed atomic functions ϕ_i^α provide the major contribution to the hyperfine interaction at nucleus i. This result follows from the nature of the hyperfine Hamiltonian which is very small everywhere except in the immediate vicinity of the nucleus. In calculating $|\psi(\mathbf{r}_i)|^2$ for a given nucleus i, it is therefore necessary to include in ψ only Φ and those S-state orbitals ϕ_i^α which are centered on atom i. Since $\Phi(\mathbf{r})$ is a slowly varying function of position, the overlap integral $\langle\phi_i^\alpha|\Phi\rangle$ can be approximated by

TABLE II. Hyperfine parameters (a_j and b_j) and the corresponding linear combination of atomic orbitals–molecular orbitals (LCAO-MO) wave-function coefficients calculated from the observed hyperfine constants for the atom sites in the vicinity of the donor under study.

Atomic site	No. of atoms	a (MHz)	b	α_j^2	β_j^2	η_j^2	$N\eta_j^2$
^{69}Ga 1NN	4	27.64	7.16	0.07	0.93	0.0520	0.21
^{69}Ga 3NN	12	16.73	0.65	0.34	0.66	0.0066	0.08
^{69}Ga 5NN	16	7.56		1.0		0.0010	0.016
^{69}Ga 7NN	16	6.68		1.0		0.0009	0.014
^{31}P 2NN	12	35.55	0.32	0.75	0.25	0.0042	0.05
^{31}P 4NN	6	16.14	0.08	0.97	0.03	0.0015	0.01
^{31}P 6NN	24	6.70		1.0		0.0006	0.014
^{31}P 8NN	8	6.02		1.0		0.0005	0.004

$$\langle \phi_i^\alpha | \Phi \rangle \simeq \Phi(\mathbf{r}_i) \int \phi_i^\alpha \, dV \ . \tag{9}$$

Combining Eqs. (8) and (9) we obtain

$$|\psi(r_i)|^2 \simeq G_i N^2 |\Phi(r_i)|^2 \ , \tag{10}$$

where

$$G_i = \left| 1 - \sum_\alpha \phi_i^\alpha(0) \int \phi_i^\alpha \, dV \right|^2 \ . \tag{11}$$

In our analysis, the measured isotropic hyperfine constants shown in Table II were used to determine the electron density $|\psi(r_i)|^2$ at each of the nearly nuclei i. G_i was calculated by using self-consistent Hartree-Fock functions for the Ga^0 and P^0 ions where the sum was over only the filled core orbitals ($1S,2S$ for P, $1S,2S,3S$ for Ga).[23] We then determined $|N\Phi(r_i)|$ and the values for the shells analyzed are given in Table III and in Fig. 10. We note in the figure that this method of analysis does indeed appear to reflect an enhanced concentration on the P sublattice, perhaps a residual influence of the X_1 valleys, although the effect is not large. The average radial dependence is explained well by a simple exponential dropoff as indicated. Volume integrating this averaged $[N\Phi(r)]^2$ gives the normalization factor $N \approx 0.89$, a reasonable value. Using this value of N, the normalized $|\Phi(r_i)|$ were also estimated and the results are included in Table III. In Fig. 10, the appropriate vertical scale for $|\Phi(r)|$ has also been included.

In order to extract an estimate of the binding energy of the defect wave function the following was argued. We expect that the wave function at large distance from the central cell should drop off exponentially with a rate reflecting the binding energy of the unpaired electron. We approximate the envelope wave function as that of the $1S$ hydrogen atom state in a uniform medium of dielectric constant ϵ_{eff}. This problem has the simple solution[24]

$$\psi_{1S} = \frac{1}{(\pi a_0^3)^{1/2}} e^{-r/a_0} \tag{12}$$

with binding energy

$$E = m^* e^4 / 2\epsilon_{\text{eff}}^2 \hbar^2 \tag{13}$$

TABLE III. Estimated values of the envelope function for the donor in GaP:O at several atomic sites.

Atom sites i	$\lvert N\Phi(\mathbf{r}_i)\rvert$ (a.u.)	$\lvert\Phi(\mathbf{r}_i)\rvert$ (a.u.)
$Ga^0, G_i = 470.56$		
1NN (r=4.46 a.u.)	0.00746	0.00840
3NN (8.54 a.u.)	0.00582	0.00654
5NN (11.23 a.u.)	0.00383	0.00430
7NN (13.38 a.u.)	0.00363	0.00408
$P^0, G_i = 141.59$		
2NN (r=7.28 a.u.)	0.01112	0.01249
4NN (10.30 a.u.)	0.00747	0.00840
6NN (12.62 a.u.)	0.00489	0.00550
8NN (14.57 a.u.)	0.00444	0.00500

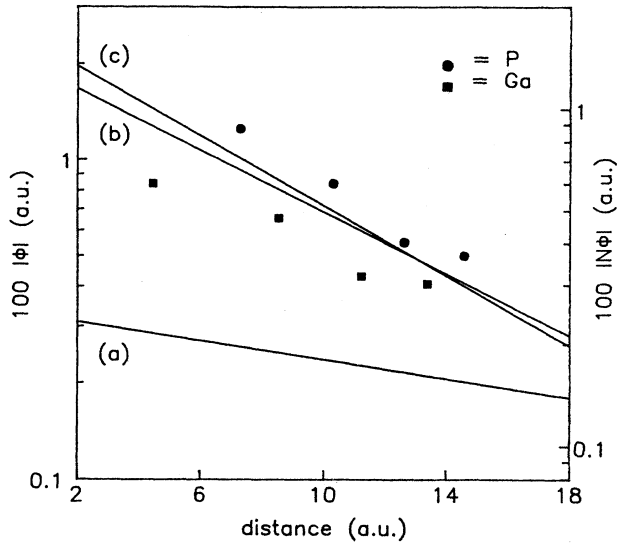

FIG. 10. Envelope function for the unpaired electron of the defect under study showing the experimentally determined values for the P and Ga shells. Normalized $1S$ hydrogenic wave functions are shown with (a) effective-mass Bohr radius $a_0 = 30.9$ a.u. resulting from $\epsilon_{\text{st}} = 10.8$ and $m^* = 0.35 m_e$; (b) $a_0 = 9.0$ a.u., resulting from $\epsilon_{\text{op}} = 9.0$, and $m^* = m_e$, and (c) best match $a_0 = 7.9$ a.u.

and a Bohr radius

$$a_0 = \frac{\epsilon \hbar^2}{m^* e^2} = \frac{\hbar}{\sqrt{2m|E|}} \ . \tag{14}$$

First consider the solution of Eq. (12) for an effective-mass-like wave function with $m^* = 0.35m$ (Ref. 25) and with the static dielectric constant[25] $\epsilon_{\text{st}} = 10.8$ appropriate for a large orbit wave function. The result is shown as curve a in Fig. 10. This wave function has a binding energy of 0.04 eV and an effective Bohr radius a_0 of 30.9 a.u. The predicted amplitude on the nearest neighbors and dropoff rate for the defect envelope function are clearly much less than the experimentally observed values. Next consider the solution with the free-electron mass and the optical dielectric constant $\epsilon_{\text{op}} = 9.0$ (Ref. 25) more appropriate to a deeper state. The resulting binding energy is 0.17 eV with $a_0 = 9.0$ a.u. The wave function as shown in Fig. 10 [curve (b)] is very close to the experimental results. The best match to the experimental data, given by curve (c) in Fig. 10 corresponds to $a_0 = 7.9$ a.u. With Eq. (14) this suggests a binding energy of ~ 0.22 eV, reflecting presumably a small additional central cell effect.[26] To our knowledge this does not correspond to any known level of oxygen in GaP (Ref. 6) or of the other group-VI donor-energy levels of S, Se, and Te at 0.110, 0.109, and 0.095 eV below the conduction band.[27]

E. Discussion

Ordering the shells as we have done in simple monotonic order versus distance serves, therefore, to give a

consistent picture for the defect. However, we must be careful. For example, a pure effective-mass X_1 state predicts wave-function probability density oscillations on the sequential P shells of 3:1:3:1, etc. Although we have argued that it cannot be a pure effective-mass state, residual effects of these oscillations could be present. We have a few good benchmarks: On the P sublattice, we have the C_{2v} site which has been assigned to the six-atom second P shell. This would be an X_1 predicted "3-density" shell and the probability of error is therefore small. (The next shell of this symmetry, also of 3-intensity, is at twice the separation and, according to Fig. 10, the envelope has decreased by over a factor of 4.) The first-, third-, and fourth-P-nearest-neighbor shells, however, all have C_{1h} symmetry, the first and third having an X_1 predicted "1-density" and the fourth, 3-density. There is the danger here of misordering. However, we believe the nearest shell is at least correctly identified. Otherwise the envelope function would not decrease versus r. These arguments suggest therefore that the first two P shells at least are correctly identified. On the Ga sublattice we can argue again that the first two are correctly identified because of their different C_{3v} and C_{1h} symmetries plus the progressively decreasing quadrupole interaction which reflects the electric field gradient produced by the core. The last two of each sublattice therefore could be misordered but it is clear from Fig. 10 that would not affect the conclusions significantly.

The substantial wave-function concentration on the Ga sublattice and the apparent lack of significant radial oscillations argue strongly against substantial X_1 effective-mass character in the wave function. Also the sharp ENDOR transitions for each shell and overall T_d symmetry indicate an electronic state of A_1 symmetry, not $1S(E)$. As pointed out earlier, the $1S(E)$ state is doubly degenerate and strains would mix the two to provide large random departures from equal electron density on each atom of a given shell. Finally, our state is deep $\sim$0.22 eV, inconsistent with the estimate for the $1S(E)$ state of $\sim$0.05 eV[2], as shown in Fig. 2.

Still, we have estimated that the wave function is centered on the P sublattice and its negative ENDOR signal has so far been reported only for GaP:O. We believe that it is associated with the donor state of a defect because of its isotropic $g \approx 2$. An acceptor state at $E_v + 0.22$ eV should have considerable orbital angular momentum admixed into it with a corresponding g value significantly different from 2. If we had been able to determine the relative signs of Q_i' and A_i we could have deduced the sign of the charge of the core of the defect, providing a direct test of its donor or acceptor character. This continues to suggest identification with substitutional oxygen in its donor state. Possibilities that should perhaps be considered are excited $1S(A_1)$ states made up from higher-lying subsidiary conduction-band minima (Γ, L, etc.) as has been proposed for donors in $Al_xGa_{1-x}As$ (Ref. 28) or the $2S(A_1)$ state from X_1, its depth resulting from a large central-cell effect as has been found for the $1S(A_1)$ ground state of oxygen.[2] It would clearly be highly desirable to study a sample doped with the magnetic isotope ^{17}O.

V. CONCLUSIONS

We have investigated a donor in GaP:O which gives rise to a quenching ODMR signal on both oxygen-related near-infrared photoluminescence bands by resolving its ligand hyperfine structure with the ODENDOR technique. This ODMR signal was assigned recently by Lee *et al.*[13] to the shallow effective-mass-like $1S(E)$ excited state of neutral oxygen. We have established that the wave function is centered on the P sublattice. It has full T_d symmetry indicating a defect wave function of A_1 symmetry. It has considerable hyperfine interaction on the Ga neighbor shells and $\sim$40% of the donor electron wave-function distribution has been accounted for between the first- and eighth-nearest-neighbor shells. An orthogonalized envelope-function analysis was performed and the observed dropoffs for both the P and Ga shells are well matched with a free-electron mass hydrogenic $1S$ wave function with a binding energy of $\sim$0.22 eV. Therefore the donor is rather deep which in turn means that the quenching ODMR resonance does not result from the effective-mass-like $1S(E)$ state of neutral oxygen.

The identity of the donor is still unknown. Since the binding energy ($\sim$0.22 eV) does not correspond to any known donor level associated with oxygen in GaP a number of possibilities are suggested. (i) The donor is not oxygen. Near-band-gap PL is also observed from this sample indicating the presence of the shallow group-VI donors S, Se, and Te. Their known binding energies, $\sim$0.1 eV, however, also do not match. (ii) The resonance occurs in an excited $1S(A_1)$ state made up from higher-lying subsidiary minima (Γ,L) or from the $2S(A_1)$ state associated with X_1. At this point those various suggestions cannot be distinguished.

ACKNOWLEDGMENTS

Discussions on the envelope-function calculations with W. B. Fowler and F. S. Ham are gratefully acknowledged. The authors are particularly indebted to W. A. Barry, who wrote the computer algorithms used to fit the angular-dependence data. The sample used in the study was provided by K. M. Lee of AT&T Bell Laboratories, Murray Hill, NJ. This research was carried out under the support of the National Science Foundation Grant No. DMR-85-20269.

[1]P. J. Dean, C. H. Henry, and C. J. Frosch, Phys. Rev. **168**, 812 (1968).
[2]P. J. Dean and C. H. Henry, Phys. Rev. **176**, 928 (1968).
[3]H. Kukimoto, C. H. Henry, and F. R. Merritt, Phys. Rev. B **7**, 2486 (1973).
[4]C. H. Henry, H. Kukimoto, T. L. Miller, and F. R. Merritt, Phys. Rev. B **7**, 2499 (1973).
[5]T. N. Morgan, Phys. Rev. B **29**, 5667 (1984).
[6]P. J. Dean, in *Deep Centres in Semiconductors,* edited by S. T. Pantelides (Gordon and Breach, New York, 1986), Chap. 4.
[7]S. Toyotomi and K. Morigaki, J. Phys. Soc. Jpn. **29**, 800 (1970).
[8]M. Gal, B. C. Cavenett, and P. Smith, Phys. Rev. Lett. **43**, 1611 (1979).
[9]M. Gal, B. C. Cavenett, and P. J. Dean, J. Phys. C **14**, 1507 (1981).
[10]K. M. Lee, in *Defects in Electronic Materials,* Symposium Proceedings of the Materials Research Society, edited by Michael Stavola, S. J. Pearton, and G. Davies (MRS, Pittsburgh, 1988) Vol. 104, p. 449.
[11]M. Godlewski and B. Monemar, Phys. Rev. B **37**, 2752 (1988).
[12]J. F. Donegan, D. Y. Jeon, and G. D. Watkins (unpublished).
[13]K. M. Lee, L. C. Kimerling, and M. D. Sturge, in *Microscopic Identification of Defects in Semiconductors,* Symposium Proceedings of the Materials Research Society, edited by N. M. Johnson, S. G. Bishop, and G. D. Watkins (MRS, Pittsburgh, 1985) Vol. 46, p. 319.
[14]K. M. Lee, Rev. Sci. Instrum. **53**, 702 (1982).
[15]*Handbook of Chemistry and Physics,* 65th ed., edited by R. C. Weast (CRC, Boca Raton, 1985), p. E66.
[16]J. B. Mullin, B. W. Straughan, and W. S. Brickall, J. Phys. Chem. Solids **26**, 782 (1965).
[17]F. Mehran, T. N. Morgan, R. S. Title, and S. E. Blum, Phys. Rev. B **6**, 3917 (1972).
[18]G. Feher, Phys. Rev. **114**, 1219 (1959).
[19]G. D. Watkins and J. W. Corbett, Phys. Rev. **134**, A1359 (1964).
[20]A. K. Koh and D. J. Miller, At. Data Nucl. Data Tables **33**, 235 (1985).
[21]B. S. Gourary and F. J. Adrian, Phys. Rev. **105**, 1180 (1957).
[22]B. S. Gourary and F. J. Adrian, in *Solid State Physics,* edited by F. Seitz and D. Turnbull (Academic, New York, 1960), Vol. 10, p. 127.
[23]E. Clementi and C. Roetti, At. Data Nucl. Data Tables **14**, 177 (1974).
[24]W. Kohn and J. M. Luttinger, Phys. Rev. **97**, 1721 (1955).
[25]N. Neuberger, *III-V Semiconducting Compounds,* Vol. 2 of *Handbook of Electronic Materials* (Plenum, New York, 1972).
[26]A more rigorous justification of this scaling is to consider the Whittaker functions [see E. T. Whittaker and G. N. Watson, *A Course of Modern Analysis* (Cambridge University Press, Cambridge, 1952)] which are the correct solutions in regions of space where a Coulomb potential is appropriate. The asymptotic form for large r is $\exp[-(2m^*|E|)^{1/2}r/\hbar]$ independent of the form of the potential near the origin.
[27]R. S. Title, Phys. Rev. **154**, 668 (1967).
[28]J. C. M. Henning, J. P. M. Ansems, and P. J. Raksnoer, Semicond. Sci. Technol. **3**, 361 (1988).